Arylphosphonate-Tethered Porphyrins: Fluorescence Silencing Speaks a Metal Language in Living Enterocytes**

Claudia Keil,[a] Julia Klein,[a] Franz-Josef Schmitt,[b] Yunus Zorlu,[c] Hajo Haase,*[a] and Gündoğ Yücesan*[a]

We report the application of a highly versatile and engineerable novel sensor platform to monitor biologically significant and toxic metal ions in live human Caco-2 enterocytes. The extended conjugation between the fluorescent porphyrin core and metal ions through aromatic phenylphosphonic acid tethers generates a unique turn off and turn on fluorescence and, in addition, shifts in absorption and emission spectra for zinc, cobalt, cadmium and mercury. The reported fluorescent probes p-H$_8$TPPA and m-H$_8$TPPA can monitor a wide range of metal ion concentrations via fluorescence titration and also via fluorescence decay curves. Cu- and Zn-induced turn off fluorescence can be differentially reversed by the addition of common chelators. Both p-H$_8$TPPA and m-H$_8$TPPA readily pass the mammalian cellular membrane due to their amphipathic character as confirmed by confocal microscopic imaging of living enterocytes.

Introduction

Nearly half of all cellular proteins require one or more metal ions as cofactors (transition metals to alkali and alkaline-earth metals) to perform their functions.[1] Metal ions are present in all six classes of enzymes[2] and metalloproteins assume significant roles in signal transduction.[3–6] Therefore, the distribution of metal ions in biology is very tightly regulated through a complex network of interactions ensuring proper metal ion homeostasis.[7,8] Disturbance or mutations in the metabolic pathways of metal ion homeostasis could produce significant disarray in signal transduction or impede other biochemical pathways,[3–6,9] resulting in cellular damage or even death, for example, by apoptosis,[10–12] and promote diseases such as cancer,[13] diabetes,[14–16] vascular[17] or soft tissue calcifications[18] and Alzheimer's disease.[19–21] Therefore, monitoring the concentrations of metal ions in living systems is crucial to provide diagnosis and treatment of innumerous metabolic disorders as well as to understand the mechanism of how metal ions are regulated.[22–24]

Despite the importance of metal ions in biology, there are still only a few methods to monitor free or unbound metal ion concentrations; among them, fluorescent imaging is one of the most suitable techniques.[25–27] Small-molecule fluorescent sensors could generate response upon metal binding[24,28–31] or protein and peptide-based systems mobilize fluorescent compartments to produce FRET fluorescence upon metal binding.[32–35] However, the number of such fluorescent probes is limited, and design routes to create metal ion responsive fluorescence are not yet well-established. The ideal fluorescent probe to detect metal ions should provide dynamic electronic interactions between the fluorescent core and the metal ion to cause a detectable change in fluorescence. To this end, the metal sensing unit of the fluorescent probe should be directly attached to at least one of the sp^2 carbon atoms to produce extended conjugation interacting with the target metal. In contrast, sp^3 bonded metal sensing units could carry the fluorescent tag to a targeted area without altering the fluorescent signal upon metal binding. We have recently shown that such a design strategy in extending the conjugation of the fluorescent core allows direct electronic interactions with rat bone sections, in return producing turn up fluorescence upon hydroxyapatite binding using p-H$_8$TPPA and m-H$_8$TPPA fluorescent probes,[36] with toxicity studies indicating that p-H$_8$TPPA was well tolerated by an intestinal cell line.[37]

Phenylphosphonic acid tethers provide 1.7 and 7.4 pK_a1 and pK_a2 values, respectively,[38,39] and each of the phenylphosphonic acid tethers are expected to provide −2 negative charge at physiological pH. Therefore, phosphonic acid derivatives could be used to generate ionic interactions with divalent metal ions in biological systems, but their use as metal sensing units has been neglected due to difficult and limited synthetic routes, especially due to the challenge of forming P–C bonds in conjugated fluorescent systems. Consequently, the number of aromatic phosphonic acids in the literature are still quite

[a] Dr. C. Keil, J. Klein, Prof. Dr. H. Haase, Dr. G. Yücesan
     Technische Universität Berlin,
     Chair of Food Chemistry and Toxicology
     Straße des 17. Juni 135, 10623 Berlin (Germany)
     E-mail: haase@tu-berlin.de
            yuecesan@tu-berlin.de
[b] Dr. F.-J. Schmitt
     Martin-Luther-Universität Halle-Wittenberg
     Department of Physics
     von-Danckelmann-Platz 3, 06120 Halle/Saale (Germany)
[c] Dr. Y. Zorlu
     Department of Chemistry, Faculty of Science
     Gebze Technical University
     41400 Gebze-Kocaeli (Turkey)

ChemBioChem

Communications
doi.org/10.1002/cbic.202100031

Chemistry Europe
European Chemical
Societies Publishing

limited.[39–43] To further understand the metal-induced fluorescence change observed in rat bone sections, we continued using arylphosphonic acids in Scheme 1, from left to right, 5,10,15,20-tetrakis [*m*-phenylphosphonic acid] porphyrin (*m*-H$_8$TPPA), its positional isomer 5,10,15,20-tetrakis [*para*-phenylphosphonic acid] porphyrin (*p*-H$_8$TPPA), and the ester form 5,10,15,20-tetrakis-[*p*-(diisopropoxyphosphoryl)phenyl] porphyrin (*p*-H$_8$TPPA-iPr$_8$); this time to create a differentially altered fluorescence upon binding to metal ions. For this study, we have selected a range of biologically relevant metal ions and toxic heavy metals. We have observed a wide variety of unique fluorescent responses upon binding of the fluorophores with the biologically relevant metal ions Zn, Cu, Co, Ni, Fe, Mn, Mg, Ca, and toxic metal ions Cd, Pb, Hg, and Co in Caco-2 cells. We intentionally inhibited the extended conjugation of the fluorescent core (*p*-H$_8$TPPA) and the metal ion binding by using the isopropyl diester (*p*-H$_8$TPPA-iPr$_8$), which showed no fluorescence change upon metal binding.
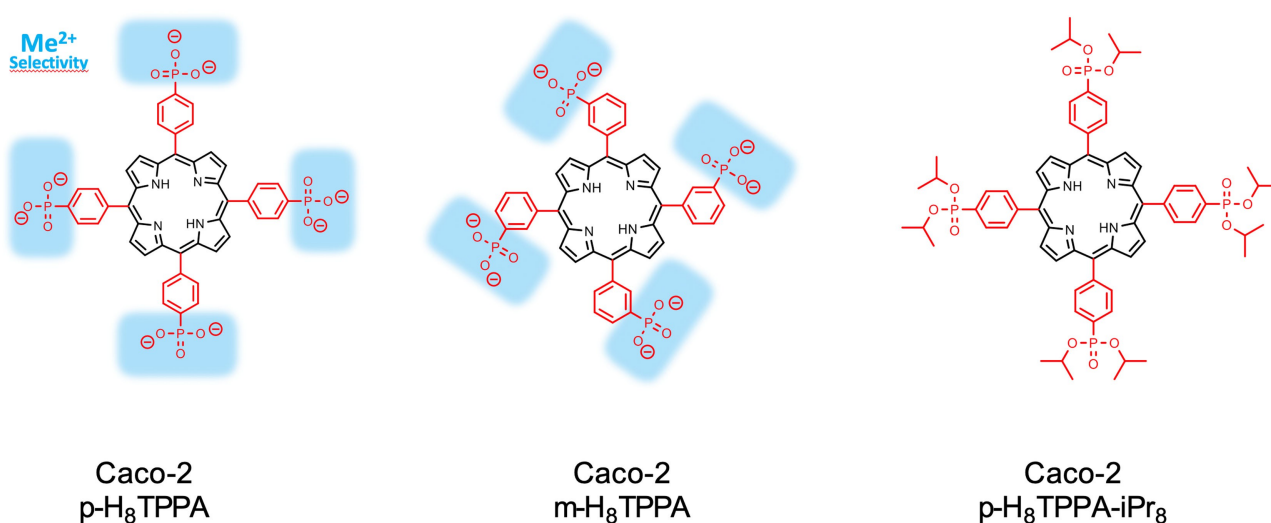
Results and Discussion

Aiming to use arylphosphonate-tethered porphyrins as real-time cellular metal fluorescence sensors, we first characterized their metal-responsiveness under cell-free conditions. *p*-H$_8$TPPA (Figure 1) and *m*-H$_8$TPPA (Figure S1 in the Supporting information), were pretreated with various bivalent metal ions at a pH close to the cellular milieu (pH 7.4) before recording absorption and fluorescence spectra. The visible absorption of both sensors in the buffer-controlled treatment showed maxima in the range of 380–430 nm, with a typical Soret peak at around 416 nm, already observed in our recent studies[36,44] and also by others.[45] Ca^{2+} or Mg^{2+} treatment did not shift the position of the Soret maximum, but slightly raised the intensity of the absorption spectrum causing a higher fluorescence, characteristic for non-ratiometric metal-ON fluorescence sensors. This observation

confirms our recent results of H$_8$TPPA and *m*-H$_8$TPPA fluorescence enhancement in the presence of calcium-hydroxyapatite phases or bones.[36] Mn^{2+}, and far more pronounced Pb^{2+}, narrowed non-ratiometrically the photon absorbing properties of *p*-H$_8$TPPA and *m*-H$_8$TPPA, thus their fluorescence dropped markedly.

The Cd^{2+}-treated sensors showed a decline of the 416 nm absorbance maximum and the appearance of a new band peaking at 434 nm. Following Co^{2+} treatment absorption spectra were less intense, plateau-shaped with a bathochromic broadening up to 434 nm. Hg^{2+}-treatment red-shifted the Soret band by approximately 30 nm. Albeit that, none of the absorption shifts led to comparable shifts in the emission bands. Despite of their restricted fluorescence intensity, the fluorescence emission patterns of all the aforementioned metal-treated arylphosphonate-tethered porphyrins seemed to be completely distinct und almost indistinguishable from the buffer-controls (Figures 1C, S1 and S3). Zn^{2+} treatment led to a declined and much more broadened Soret band in the range of 380–430 nm (Figure 1A). Still, the fluorescence emission was much lower than what would have been expected from the fluorescence excitation properties (Figure 1B and C). Thus, we assume a fluorescence quenching effect of Zn^{2+} that requires further investigation.

Steady-state fluorescence spectra of *p*-H$_8$TPPA/*m*-H$_8$TPPA-loaded Caco-2 cells exhibit a S1-fluorescence pattern with two-band emission maxima at 655 and 705 nm, almost perfectly matching the fluorescence characteristics of the sensor applied in a physiological buffer (Figure 2A). Thus, *p*-H$_8$TPPA and *m*-H$_8$TPPA seemed to pass the cellular membrane reaching the cell interior intact (Figures 2A and S2), a result further confirmed by confocal microscopic imaging of living enterocytes (Figure 2B). We further performed cellular uptake experiments implementing the detergent pluronic F-127, aiming to counterbalance the partial hydrophobic properties of the porphyrin skeleton. Yet, the amphipathic character of *p*-H$_8$TPPA and *m*-H$_8$TPPA is

Scheme 1. Structures and metal binding units of *p*-H$_8$TPPA and *m*-H$_8$TPPA

ChemBioChem

Communications
doi.org/10.1002/cbic.202100031

**Chemistry
Europe**
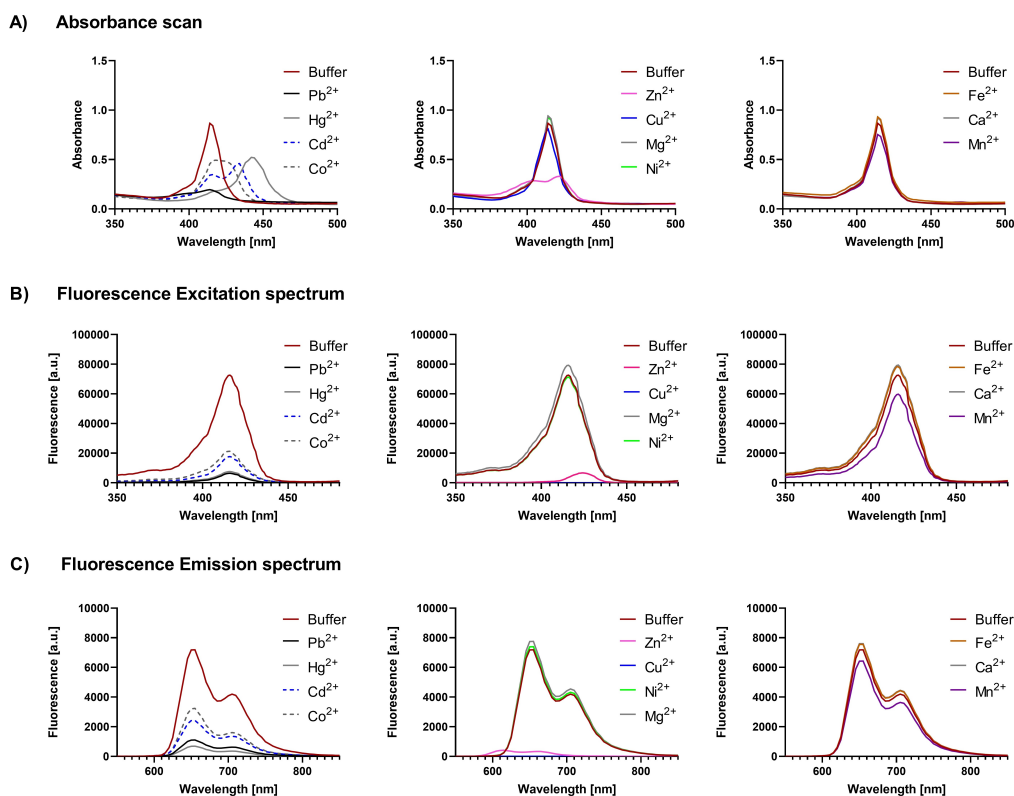European Chemical
Societies Publishing

Figure 1. Metal-dependent changes in p-H_8TPPA absorbance and fluorescence properties. 10 μM p-H_8TPPA dilutions were treated with various metal solutions (final concentration 40 μM) before recording A) absorbance, B) fluorescence excitation ($\lambda_{em} = 650$ nm) and C) fluorescence emission ($\lambda_{ex} = 415$ nm) spectra. Data are representative for three independent experiments.

sufficient to enable cellular entrance (Figure 2A). Aside from the two fluorescent arylphosphonic acids an isopropyldiester-modified variant (p-H_8TPPA-iPr$_8$), intentionally blocked for metal binding at the phosphonate moiety, was aimed for Caco-2 cell application. As seen in Figure 2C, the fluorescence emission output of p-H_8TPPA-iPr was much lower in the incubation buffer as well as in the presence of cells. The confocal microscopy pictures depict p-H_8TPPA-iPr$_8$ microcrystals of ~20 μm size, inaccessible for cellular uptake. Even the presence of the detergent pluronic did not improve the solubility of the diester in aqueous media (Figure 2C).

Addition of CuSO$_4$ caused the most pronounced effects of all metal ions tested. Upon treatment with 40 μM Cu^{2+} almost complete abrogation of p-H_8TPPA and m-H_8TPPA (final concentrations 10 μM) fluorescence was observed (Figures 1C, 3A and S1). The half maximal effective concentration for p/m-H_8TPPA fluorescence silencing was considerably lower for copper than for all the other metal cations tested (Figures 3 and S4).

Time-resolved fluorescence spectroscopy was shown to be highly efficient unraveling interaction mechanisms between fluorescent probes and their surroundings, including specific ions.[46,47] It was successfully applied to unravel structural molecular changes that are correlated with fluorescence quenching.[48,49] In particular, it allows the quantitative study of dynamic electronic interactions between the fluorescent core and the metal ion to cause a characteristic change in

fluorescence intensity and lifetime.[50–52] The time-resolved fluorescence showed a dose-dependency in the initial amplitudes of the p-H_8TPPA fluorescence decay curves for Cu^{2+} at concentrations between 0 and 8 μM (Figure 4A). Noticeably, the time constant was stable for all concentrations. The quantitative fit of the decay curves resulted in 8.3 ns fluorescence lifetime for p-H_8THPPA up to 8 μM copper dosing, so at low concentrations of CuSO$_4$ the observed quenching is purely static. At higher Cu^{2+} concentrations (10–40 μM) an increased excitation intensity and prolonged measuring time was needed to improve the signal-to-noise ratio. Under these conditions the copper quenching becomes dynamic (lifetime dropped to 1.7 ns starting at a concentration of CuSO$_4$ of 10 μM) and/or it is correlated with a molecular change (e.g., oxidation of the molecules), which induces the change of the fluorescence lifetime observed in Figure 4C. Similar behavior was observed for m-H_8TPPA, which exhibited a constant lifetime of 7.7 ns up to 8 μM CuSO$_4$ with concomitant drop of the amplitude (Figure 4B), while above this concentration a pronounced drop in lifetime was observed, resulting in 1.6 ns fluorescence decay time (Figure 4D).

The assumption of an at least partially irreversible molecule change was further supported by the observation that the copper-induced decrease in p/m-H_8TPPA fluorescence remained almost non-responsive to metal chelator (EDTA or EGTA) posttreatment, whereas for Zn^{2+} as well as Hg^{2+} quenching

ChemBioChem

Communications
doi.org/10.1002/cbic.202100031

Chemistry
Europe
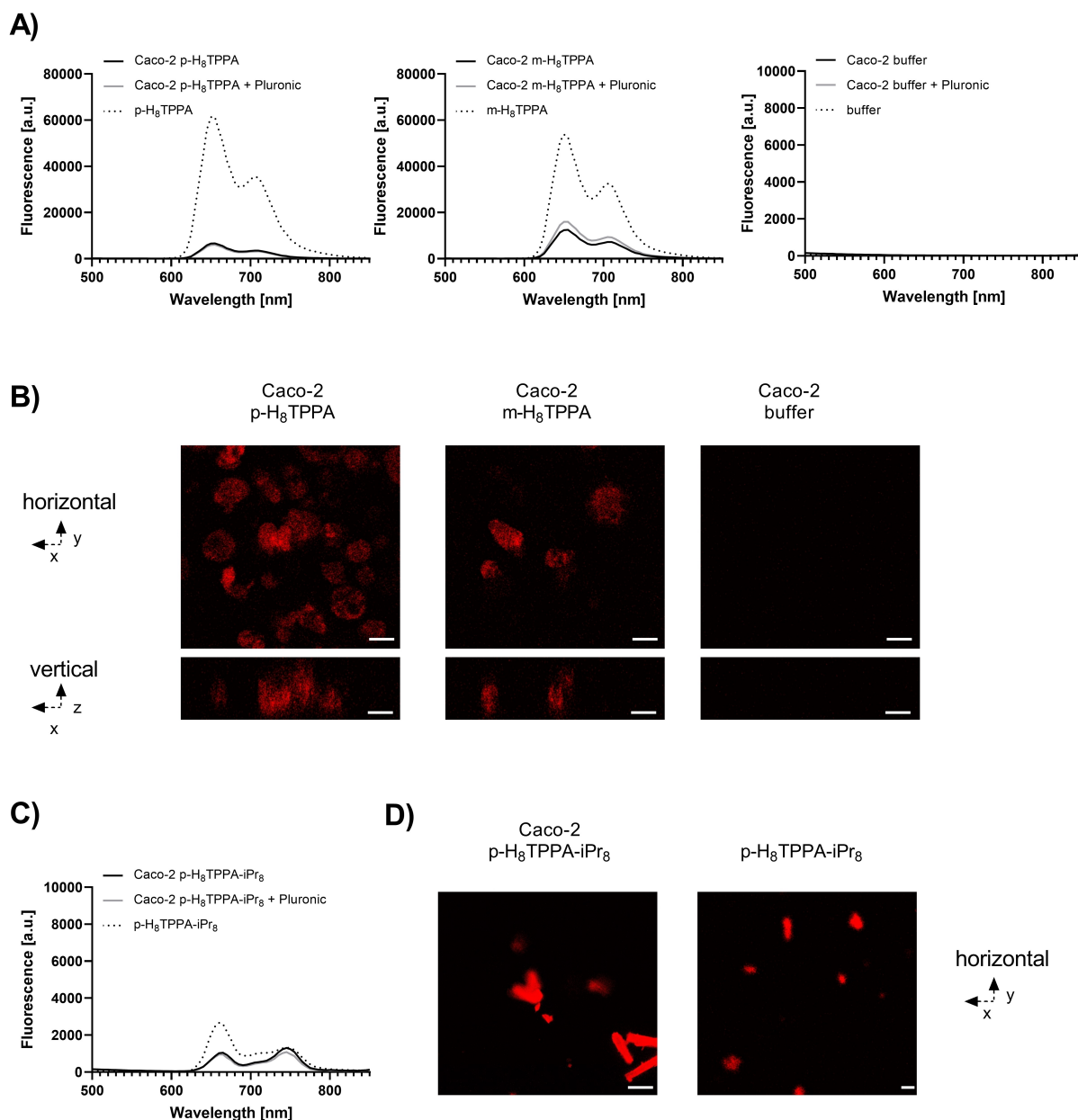European Chemical
Societies Publishing

Figure 2. Fluorescence labeling of Caco-2 enterocytes by phenylphosphonate-substituted porphyrines. Fluorescence emission spectra of Caco-2 cells exposed to A) p-H$_8$TPPA, m-H$_8$TPPA or C) the isopropyl-modified phosphonate p-H$_8$TPPA-iPr$_8$ in comparison with each of the phenylphosphonate porphyrins as 10 μM dilution in assay buffer ($\lambda_{ex} = 416$ nm). B) Confocal images of Caco-2 upon loading with p-H$_8$TPPA or m-H$_8$TPPA. D) Confocal images of p-H$_8$TPPA-iPr$_8$ in the presence or absence of Caco-2 cells. Scale bars: 10 μm. Data are representative of three independent experiments.

was reversed by both chelators (Figure 5). Quenching of p-H$_8$TPPA and m-H$_8$TPPA fluorescence was observed for Cu^{2+} and Cu$^+$, irrespective of the oxidation state of copper (Figure S5). This is of importance for future applications, given that copper is present as Cu$^+$ in the intracellular milieu, whereas the cupric state (Cu^{2+}) predominates in the systemic blood circulation.[9,53]

When present within Caco-2 cells, p-H$_8$TPPA/m-H$_8$TPPA fluorescence remained stable upon extracellular addition of 50 μM FeSO$_4$ (Figure 6A), whereas *in vitro* both sensors were slightly enhanced by iron treatment (Figure 1). For Cd^{2+}, Cu^{2+}, Hg^{2+} Mn^{2+}, Pb^{2+} and Zn^{2+} a 50 μM incubation concentration

was already shown to be sufficiently high to admit quantitative metal ion delivery into Caco-2.[54–56] The arylphosphonate-tethered porphyrin sensors introduced into the human enter-ocytes record these incoming metal cations in a fluorescence silencing language (Figures 6A–C and S6).

The strong and rapid decline in Caco-2 p-H$_8$TPPA/m-H$_8$TPPA fluorescence upon Cu-exposure was somewhat surprising (Figure 6A) keeping in mind the tight copper buffering ability of the cellular metallochaperons Atox1 (antioxidant 1 copper chaperone), Ccs (copper chaperone for superoxide dismutase), Cox17 (cytochrome c oxidase copper chaperone) and gluta-
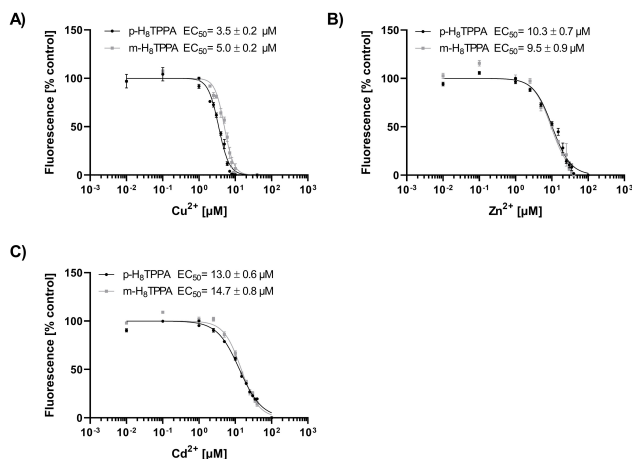
ChemBioChem

Communications
doi.org/10.1002/cbic.202100031

Chemistry Europe
European Chemical
Societies Publishing

Figure 3. Fluorescence titration of p-H$_8$THPPA and m-H$_8$TPPA with metal cations. 10 μM solutions of p-H$_8$TPPA or m-H$_8$TPPA were treated with increasing quantities of metal cations followed by detection of fluorescence emission ($\lambda_{ex} = 416$ nm, $\lambda_{em} = 650$ nm). Data are means ± S.E.M. of at least $n = 3$ independent experiments. Sigmoidal dose–response curves were fitted by nonlinear regression, and the resulting EC$_{50}$ values are indicated.
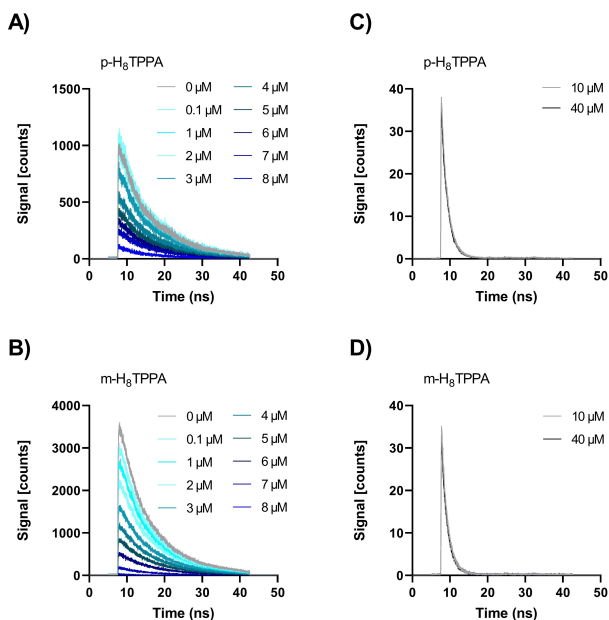

Figure 4. Fluorescence decay curves of p-H$_8$THPPA and m-H$_8$TPPA in the presence of CuSO$_4$. Time-resolved fluorescence was measured on p-H$_8$THPPA and m-H$_8$TPPA (each 10 μM) in the presence of various amounts of CuSO$_4$ between 0 and 40 μM. CuSO$_4$ was admixed until the actual cupric concentration was reached. Then samples were gently mixed and incubated for 60 s before time-correlated single-photon counting was performed. C), D) For 10 and 40 μM CuSO$_4$, the excitation intensity was enhanced by a factor of 8, and measuring time was prolonged by a factor of 10 to improve signal/noise output. Data shown in (C) and (D) are scaled differently for direct comparison. Data are representative of one out of three independent experiments.
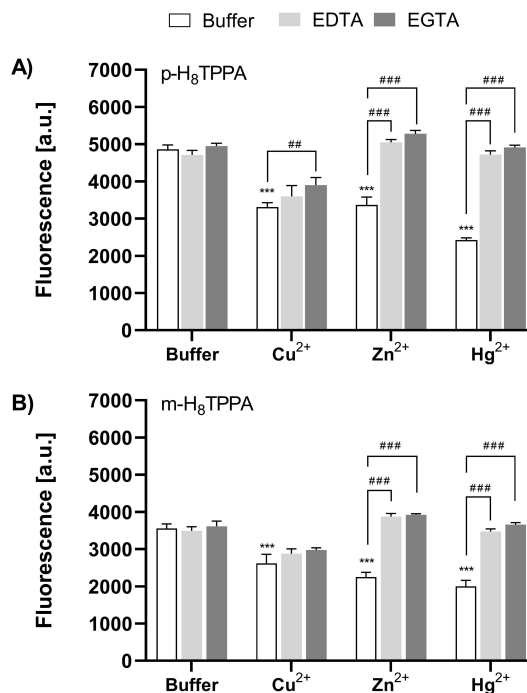
Figure 5. Reversibility of p-H$_8$THPPA and m-H$_8$TPPA metal complexation. Fluorescence of p-H$_8$THPPA or m-H$_8$TPPA solutions pretreated with metal cations upon addition of 50 equivalents of EDTA or EGTA ($\lambda_{ex} = 416$ nm, $\lambda_{em} = 650$ nm). Data are means ± S.E.M. of $n = 3$ independent experiments. Statistically significant differences from buffer incubation (*** $p < 0.001$; two-way ANOVA/ Tukey post hoc test) or from metal cation treatment (## $p < 0.01$; ### $p < 0.001$; two-way ANOVA/ Tukey post hoc test) are indicated.

therefore unable to ensure its correct sequestration. Alternatively, the phenylphosphonic acid porphyrin sensors might detect intracellular protein-complexed copper in addition to free Cu$^+$ ions. The same applies to Zn (Figure 6A). The free intracellular zinc concentration estimated with the fluorescent sensor Zinpyr-1 in Caco-2 cells treated with 50 μM ZnSO$_4$ was approximately 2 nM.[58] This is several orders of magnitude lower than the concentration required for fluorescence quenching of the phosphonate porphyrins in vitro (Figure 3B). Irrespective of the actual species causing p-H$_8$TPPA/m-H$_8$TPPA quenching, these probes are promising tools to monitor alterations of essential and toxic metals in human body fluids, cell and tissue samples during various life stages and in disease.

Conclusion

Our design strategy of extending the conjugation of fluorescent core via sp^2 bonded phosphonic acids was successful in generating unique metal-responsive fluorescent behavior for each of the studied metal ions. Therefore, as a new class of non-toxic fluorophores, phenylphosphonic acid-functionalized porphyrins provide an expandable and engineerable platform for the development of improved, targeted fluorescence sensors suitable for in vivo applications to determine and visualize metals in tissues during disease progression. This is of

thione (intracellular GSH concentration around 10 mM), balancing the pool of cellular labile copper in the femtomolar range.[9,57] It can be hypothesized that cellular homeostasis was overburdened by a supraphysiological amount of copper and
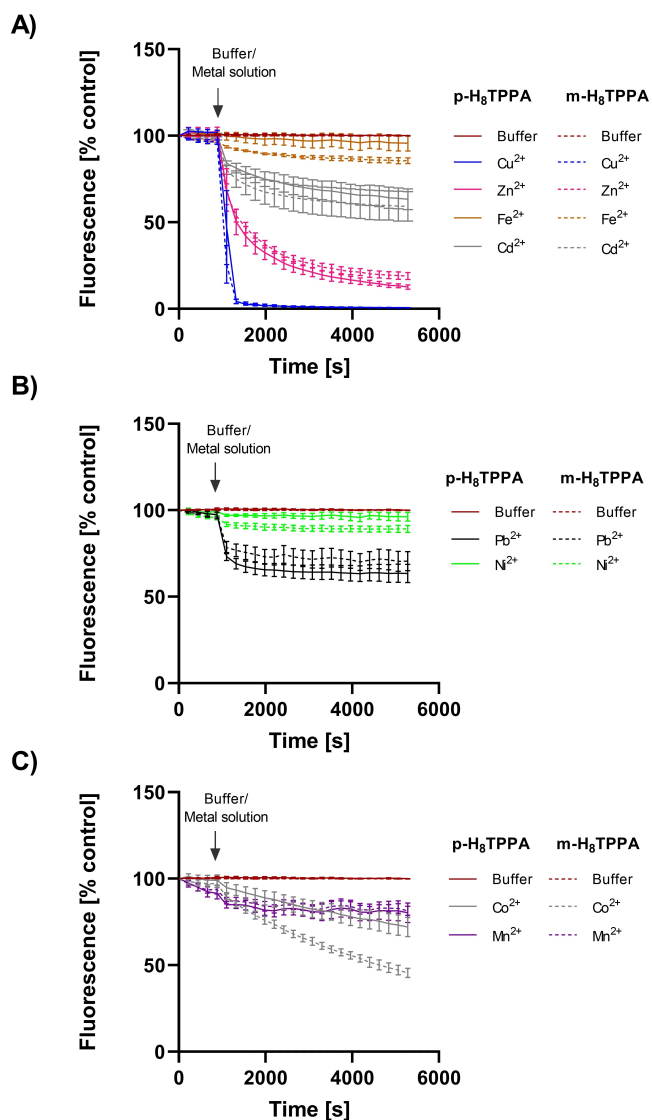
Figure 6. Live-cell sensing of metal uptake into Caco-2 enterocytes with *p*-H$_8$THPPA and *m*-H$_8$TPPA. Caco-2 cells were loaded with *p*-H$_8$THPPA or *m*-H$_8$TPPA, and the fluorescence was recorded at 3 min intervals ($\lambda_{ex} = 416$ nm, $\lambda_{em} = 650$ nm). Fifteen minutes after the start of the experiment (arrows), metal cation solutions (final concentration 50 µM) or buffer (control) were added, and the fluorescence measurement was continued. Data are means ± S.E.M. of $n = 3$ independent experiments.

utmost importance for diagnostics and in the development and translation of therapeutics for heavy metal intoxication as well as diseases associated with alterations in the homeostasis of essential metal ions.

Acknowledgements

Conflict of Interest

The authors declare no conflict of interest.

[1] K. J. Waldron, J. C. Rutherford, D. Ford, N. J. Robinson, *Nature* **2009**, *460*, 823–830.
[2] C. Andreini, I. Bertini, G. Cavallaro, G. L. Holliday, J. M. Thornton, *J. Biol. Inorg. Chem.* **2008**, *13*, 1205–1218.
[3] J. Martínez-Fábregas, S. Rubio, A. Díaz-Quintana, I. Díaz-Moreno, M. Á. De la Rosa, *FEBS J.* **2011**, *278*, 1401–1410.
[4] T. Kambe, T. Tsuji, A. Hashimoto, N. Itsumura, *Physiol. Rev.* **2015**, *95*, 749–784.
[5] H. Haase, L. Rink, *BioFactors* **2014**, *40*, 27–40.
[6] A. Grubman, A. R. White, *Expert Rev. Mol. Med.* **2014**, *16*, e11.
[7] W. Maret, A. Wedd, *Binding, Transport and Storage of Metal Ions in Biological Cells*, Royal Society Of Chemistry, London, **2014**.
[8] J. F. Collins, *Molecular, Genetic, and Nutritional Aspects of Major and Trace Minerals*, Elsevier, **2016**.
[9] J. Kardos, L. Héja, Á. Simon, I. Jablonkai, R. Kovács, K. Jemnitz, *Cell Commun. Signaling* **2018**, *16*, 1–22.
[10] A. R. Bogdan, M. Miyazawa, K. Hashimoto, Y. Tsuji, *Trends Biochem. Sci.* **2016**, *41*, 274–286.
[11] A. E. Nielsen, A. Bohr, M. Penkowa, *Biomarker Insights* **2006**, *1*, 99–111.
[12] S. P. Yu, L. M. T. Canzoniero, D. W. Choi, *Curr. Opin. Cell Biol.* **2001**, *13*, 405–411.
[13] J. J. Mordang, A. Gubern-Mérida, A. Bria, F. Tortorella, R. M. Mann, M. J. M. Broeders, G. J. den Heeten, N. Karssemeijer, *Breast Cancer Res. Treat.* **2018**, *167*, 451–458.
[14] S. Norouzi, J. Adulcikas, S. S. Sohal, S. Myers, *J. Biomed. Sci.* **2017**, *24*, 87.
[15] J. Lowe, R. Taveira-da-Silva, E. Hilário-Souza, *IUBMB Life* **2017**, *69*, 255–262.
[16] A. R. Khan, F. R. Awan, *J. Diabetes Metab. Disord.* **2014**, *13*, 1–6.
[17] J. Voelkl, R. Tuffaha, T. T. D. Luong, D. Zickler, J. Masyout, M. Feger, N. Verheyen, F. Blaschke, M. Kuro-o, A. Tomaschitz, S. Pilz, A. Pasch, K. U. Eckardt, J. E. Scherberich, F. Lang, B. Pieske, I. Alesutan, *J. Am. Soc. Nephrol.* **2018**, *29*, 1636–1648.
[18] A. Vallejo-Illarramendi, I. Toral-Ojeda, G. Aldanondo, A. López de Munain, *Expert Rev. Mol. Med.* **2014**, *16*, e16.
[19] A. I. Bush, W. H. Pettingell, G. Multhaup, M. D. Paradis, J. P. Vonsattel, J. F. Gusella, K. Beyreuther, C. L. Masters, R. E. Tanzi, *Science* **1994**, *265*, 1464–1467.
[20] P. Zatta, D. Drago, S. Bolognin, S. L. Sensi, *Trends Pharmacol. Sci.* **2009**, *30*, 346–355.
[21] Y. Liu, M. Nguyen, A. Robert, B. Meunier, *Acc. Chem. Res.* **2019**, *52*, 2026–2035.
[22] W. Maret, *BioMetals* **2009**, *22*, 149–157.
[23] C. M. Ackerman, S. Lee, C. J. Chang, *Anal. Chem.* **2017**, *89*, 22–41.
[24] K. P. Carter, A. M. Young, A. E. Palmer, *Chem. Rev.* **2014**, *114*, 4564–4601.
[25] G. Hong, A. L. Antaris, H. Dai, *Nat. Biomed. Eng.* **2017**, *1*, 1–22.
[26] R. McRae, P. Bagchi, S. Sumalekshmy, C. J. Fahrni, *Chem. Rev.* **2009**, *109*, 4780–4827.
[27] E. J. New, V. C. Wimmer, D. J. Hare, *Cell Chem. Biol.* **2018**, *25*, 7–18.
[28] E. M. Nolan, S. J. Lippard, *Acc. Chem. Res.* **2009**, *42*, 193–203.
[29] C. J. Frederickson, *Int. Rev. Neurobiol.* **1989**, *31*, 145–238.
[30] S. C. Burdette, G. K. Walkup, B. Spingler, R. Y. Tsien, S. J. Lippard, *J. Am. Chem. Soc.* **2001**, *123*, 7831–7841.
[31] X. A. Zhang, D. Hayes, S. J. Smith, S. Friedle, S. J. Lippard, *J. Am. Chem. Soc.* **2008**, *130*, 15788–15789.
[32] T. K. Hurst, D. Wang, R. B. Thompson, C. A. Fierke, *Biochim. Biophys. Acta* **2010**, *1804*, 393–403.
[33] H. Bischof, S. Burgstaller, M. Waldeck-Weiermair, T. Rauter, M. Schinagl, J. Ramadani-Muja, W. F. Graier, R. Malli, *Cells* **2019**, *8*, 492.
[34] S. J. A. Aper, P. Dierickx, M. Merkx, *ACS Chem. Biol.* **2016**, *11*, 2854–2864.
[35] J. L. Vinkenborg, T. J. Nicolson, E. A. Bellomo, M. S. Koay, G. A. Rutter, M. Merkx, *Nat. Methods* **2009**, *6*, 737–740.
[36] Y. Zorlu, C. Brown, C. Keil, M. M. Ayhan, H. Haase, R. B. Thompson, I. Lengyel, G. Yücesan, *Chem. Eur. J.* **2020**, *26*, 11129–11134.

[37] M. Maares, M. M. Ayhan, K. B. Yu, A. O. Yazaydin, K. Harmandar, H. Haase, J. Beckmann, Y. Zorlu, G. Yücesan, *Chem. Eur. J.* **2019**, *25*, 11214–11217.

[38] K. Nagarajan, K. P. Shelly, R. R. Perkins, R. Stewart, *Can. J. Chem.* **1987**, *65*, 1729–1733.

[39] C. M. Sevrain, M. Berchel, H. Couthon, P.-A. Jaffrès, *Beilstein J. Org. Chem.* **2017**, *13*, 2186–2213.

[40] G. Yücesan, Y. Zorlu, M. Stricker, J. Beckmann, *Coord. Chem. Rev.* **2018**, *369*, 105–122.

[41] K. Siemensmeyer, C. A. Peeples, P. Tholen, F. Schmitt, B. Çoşut, G. Hanna, G. Yücesan, *Adv. Mater.* **2020**, *32*, 2000474.

[42] P. Tholen, Y. Zorlu, J. Beckmann, G. Yücesan, *Eur. J. Inorg. Chem.* **2020**, *2020*, 1542–1554.

[43] A. Schütrumpf, A. Duthie, E. Lork, G. Yücesan, J. Beckmann, *Z. Anorg. Allg. Chem.* **2018**, *644*, 1134–1142.

[44] P. Tholen, C. A. Peeples, R. Schaper, C. Bayraktar, T. S. Erkal, M. M. Ayhan, B. Çoşut, J. Beckmann, A. O. Yazaydin, M. Wark, G. Hanna, Y. Zorlu, G. Yücesan, *Nat. Commun.* **2020**, *11*, 1–7.

[45] N. Venkatramaiah, C. F. Pereira, R. F. Mendes, F. A. Almeida Paz, P. C. Tome, *Anal. Chem.* **2015**, *87*, 4515–4522.

[46] F. J. Schmitt, B. Thaa, C. Junghans, M. Vitali, M. Veit, T. Friedrich, *Biochim. Biophys. Acta Bioenerg.* **2014**, *1837*, 1581–1593.

[47] F. J. Schmitt, E. G. Maksimov, H. Suedmeyer, V. Jeyasangar, C. Theiss, V. Z. Paschenko, H. J. Eichler, G. Renger, *Photonics Nanostructures – Fundam. Appl.* **2011**, *7*, 190–195.

[48] F. Velazquez Escobar, T. Hildebrandt, T. Utesch, F. J. Schmitt, I. Seuffert, N. Michael, C. Schulz, M. A. Mroginski, T. Friedrich, P. Hildebrandt, *Biochemistry* **2014**, *53*, 20–29.

[49] M. Vitali, D. Bronzi, A. J. Krmpot, S. N. Nikolić, F. J. Schmitt, C. Junghans, S. Tisa, T. Friedrich, V. Vukojević, L. Terenius, F. Zappa, R. Rigler, *IEEE J. Sel. Top. Quantum Electron.* **2014**, *20*, 344–353.

[50] J. Märk, F.-J. Schmitt, C. Theiss, H. Dortay, T. Friedrich, J. Laufer, *Biomed. Opt. Express* **2015**, *6*, 2522–2535.

[51] J. Märk, F.-J. Schmitt, J. Laufer, *J. Opt.* **2016**, *18*, 054009.

[52] V. Tejwani, F. J. Schmitt, S. Wilkening, I. Zebger, M. Horch, O. Lenz, T. Friedrich, *Biochim. Biophys. Acta Bioenerg.* **2017**, *1858*, 86–94.

[53] M. C. Linder, *Metallomics* **2016**, *8*, 887–905.

[54] A. Rossi, R. Poverini, G. Di Lullo, A. Modesti, A. Modica, M. L. Scarino, *Toxicol. in Vitro* **1996**, *10*, 27–31.

[55] D. I. Bannon, R. Abounader, P. S. J. Lees, J. P. Bressler, *Am. J. Physiol. Cell Physiol.* **2003**, *284*, 44–50.

[56] M. Vázquez, M. Calatayud, D. Vélez, V. Devesa, *Toxicology* **2013**, *311*, 147–153.

[57] T. D. Rae, P. J. Schmidt, R. A. Pufahl, V. C. Culotta, T. V. O'Halloran, *Science* **1999**, *284*, 805–808.

[58] M. Maares, C. Keil, J. Koza, S. Straubing, T. Schwerdtle, H. Haase, *Int. J. Mol. Sci.* **2018**, *19*, 2662.